Weakly coupled synthetic antiferromagnetic nanodiscs with perpendicular magnetic anisotropy for lab-on-chip devices

Emma N. Welbourne,[1, a)] Tarun Vemulkar,[1] Dorothée C. M. C. Petit,[1] and Russell P. Cowburn[1]
Department of Physics, Cavendish Laboratory, University of Cambridge, JJ Thomson Avenue, Cambridge, CB3 0HE, United Kingdom

(Dated: 23 August 2021)

Synthetic antiferromagnetic particles with perpendicular magnetic anisotropy offer a highly desirable platform for use in fluidic applications. This work illustrates their high level of switching field tunability and demonstrates the ability to use particle design to overcome unfavourable hysteretic changes during patterning to manufacture functional, low switching field nanodiscs. This makes them ideal candidates for lab-on-chip technologies, such as microfluidic sorting or detection devices.

The use of magnetic particles in biological and other fluidic environments has become increasingly widespread, with applications including cancer therapy, drug delivery, contrast agents, and tissue engineering[1,2]. It is beneficial to be able to tailor the particles to an individual situation, to maximise efficacy and efficiency. Therefore, engineering particles that allow for flexibility in design is highly desirable. When designing a magnetic particle for a particular application, there are a number of characteristics that should be considered to optimise efficacy. This includes stability in fluid, such that they do not agglomerate, and tunability of properties. Such properties include particle size, magnetic moment, and switching field.

Thus far, superparamagnetic nanoparticles (SPNPs) have been major candidates for biological applications[1–3]. The chemical synthesis used to manufacture SPNPs is simple and has been successfully commercialised. The main disadvantage of SPNPs is their simplistic magnetic state, which limits their tunability in switching field or moment. Despite a zero remanence state, SPNPs may agglomerate due to their high susceptibility[4,5] or their colloidal state, without significant engineering[5–9]. Magnetic-vortex microdiscs (MVMDs) have also been employed in biological applications—favoured for a high moment and relatively easy fabrication[10–13]. These particles also exhibit zero remanence, and have low susceptibility, limiting agglomeration[12]. However, MVMDs again offer minimal tunability. In-plane synthetic antiferromagnetic (SAF) particles offer a higher level of tunability than SPNPs and MVMDs. They too exhibit zero remanence, however, they have been shown to self-magnetise if their susceptibility is too high[4,12].

Perpendicularly magnetised (PM) SAF thin films have been demonstrated as highly tunable magnetic systems, with a number of desirable characteristics for applications in liquid[14]. This includes: a zero moment, antiparallel (AP) remanence state and low susceptibility, which prevent particle agglomeration; a variable and potentially high saturation magnetisation; sharp and tunable switching; and an easy axis of magnetisation with high anisotropy, which allows for efficient transduction of torque from an applied field. The ability to remotely activate and efficiently produce torque from PM SAF particles has been demonstrated as an effective means for a mechanical destruction cancer therapy[15]. Alongside this, these particles display unique magento-mechanical behaviour in liquid[16], which makes them interesting candidates for a variety of applications involving mechanical actuation or self-assembly.

In the PM SAF system, the switching field is a function of the Ruderman-Kittel-Kasuya-Yosida (RKKY) coupling field[17]. This is established and tuned by the thicknesses of the interlayer motif $Pt/Ru/Pt$[18–21], which is inserted between two ferromagnetic (FM) layers. The Ru thickness provides coarse tuning[18,20], while the Pt thickness offers a finer level of tuning[21]. The ability to finely control the switching, or activation field, of PM SAF particles is particularly useful in sorting or detection applications, especially if multi-plexing is desired. Thus far, the prevailing method for these applications in lab-on-chip devices is magnetofluidics[22]. The more complex and tunable magnetic properties of PM SAF discs could provide some added benefits, with not only controllable switching, but also clean access to increasing moment (without significantly affecting size or aspect ratio)[14], efficient access to torque for applications requiring mechanical rotation[15,23], and a planar shape to maximise the capturing of the near field interaction[24].

Recently, a fabrication method was devised for thin film based particles that maximise the conservation of key magnetic properties, and provide the ability to manufacture a high yield of well-defined discs in a wide range of sizes[25]. We will use this method to explore the capacity for creating robust PM SAF nanodiscs with a range of switching fields for fluidic applications. First, we will assess the effect of the patterning process on the PM SAF system, as we translate continuous thin films into nanodiscs. By exploring both fine and coarse tuning of the RKKY coupling, we demonstrate that the use of the 2nd strongest AF coupling peak (2 nm Ru[20]), in combination with ultrathin Pt, allows access to functional PM SAF nanodiscs that exhibit relatively low switching fields, whilst retaining an AP remanence state. These types of particle are crucial for fluidic applications in

[a)]em511@cam.ac.uk

which it is challenging to apply strong magnetic fields. This is highly relevant to lab-on-chip technologies, where for practicality and cost effectiveness it is desirable to keep applied field strength low. This includes point-of-care microfluidic devices for the sorting or detection of analytes or other biological species[24].

A PM SAF thin film is a multilayer heterostructure. The films in this work are described by the general form $Ta/Pt/CoFeB/Pt/Ru/Pt/CoFeB/Pt/Ta$, as shown in Figure 1(a). The magnetic properties of a PM SAF are governed by interfacial interactions: spin-orbit coupling between the Pt and CoFeB drives the perpendicular magnetic anisotropy (PMA)[26], and the antiferromagnetic (AF) RKKY coupling is generated by the Ru interlayer and mediated by the Pt interlayers[18–21]. In addition, the nucleation and propagation of domains during magnetic transitions are controlled by layer defects (see Section S1 of the supplementary material for more information on the structure and transitions of PM SAFs). Such defects are associated with the deposition of the heterostructure, e.g. local changes in the thickness in the metallic layers, increased waviness in the in the layer structure, or local atomic mixing at a layer interface. PM SAFs are therefore highly sensitive to any change in the stack layers or interfaces: any alteration to the distribution of defects in the multilayer affects the magnetic properties and alters the hysteresis. Previous work demonstrated the necessity of choosing underlayers and sacrificial layers that have a limited effect on the roughness of the stack, and thus the magnetic hysteresis[25,27]. It is also important to understand how the patterning process might affect the stack conditions or defect distribution, and hence the magnetic state of PM SAF nanodiscs.

This work uses the nanodisc fabrication method outlined in a previous study[25]: nanosphere lithography is used to create a mask across the surface of a thin film, which is then ion milled to "cut out" disc shaped particles (see Section S2 in the supplementary material for more detail). The ion milling step utilises accelerated Ar ions to bombard the film, which has been shown to cause significant modification of magnetic multilayer properties[28]. Firstly, a rise in temperature during milling can disrupt the interfaces through atomic diffusion[29–32].

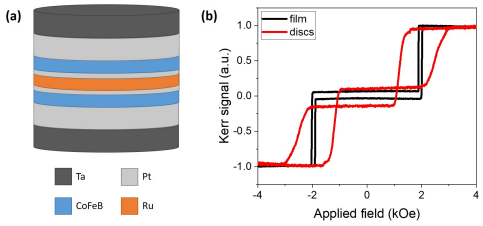

FIG. 1. (a) A schematic of our PM SAF multilayer stack. (b) Easy axis MOKE hysteresis loops of a PM SAF film and nanodiscs.

Secondly, the bombarding ions can create defects in multiple ways[28,33,34]: Ar ion implantation, sputtering away of stack atoms or mixing of stack atoms. If the induced defects are on the length scale that is associated with domain wall dynamics[35], this could alter domain nucleation or pinning behaviour.

The inherent reduction in structure size—from continuous film to nanostructures—is also a source of change in defect distribution, and thus hysteresis[36,37]. Firstly, the patterning process significantly increases the edge-to-area ratio, which can introduce additional defects[38]. This is particularly prevalent in nanostructures patterned via ion milling, as the process can cause edge damage, which induces edge nucleation processes[38]. Secondly, the patterning of a thin film into nanodiscs reduces the likelihood of an original nucleation defect being present inside the structure. This can change the switching field of an individual nanodisc, but will also create a spread in magnetic behaviour across the population[36,37]. This has previously been found in ferromagnetic nanostructures with PMA, where the switching field distribution was explained by a distribution of intrinsic anisotropy[36]. An additional source of hysteretic change related to the significant change in structure size is magnetostatic coupling: FM coupling is introduced between the dipolar magnetic fields of the CoFeB layers (predominantly within particles)[39,40]. The main consequence of this effect is a decrease in coupling, which should be relatively consistent across a population of particles. However, we calculated that these effects are too small to account for the changes observed here—see Section S3 of the supplementary material.

The summation of these effects is evident in Figure 1(b), which presents the magneto-optical Kerr effect (MOKE) hysteresis loops of a typical PM SAF stack before and after its patterning into 500 nm discs. Here, and throughout our work, we defocused the MOKE laser so as to sample a larger portion of the discs at once. The two most significant changes to the magnetic behaviour are the increase in coercivity and loss of sharp switching from film to discs. Both of these changes in hysteresis are attributed to a change in the defect distribution (both an increased number and variation in defects) across the population of nanodiscs. Additional analysis on the effect of patterning on PM SAF hysteresis, with reference to nanodisc size, can be found in Section S3 of the supplementary material. There are a few additional methods which could be employed to improve uniformity in the magnetic properties of our nanodiscs, including reduced deposition pressure[41], post-annealing[42],and editing of the composition of CoFeB[43,44]. However, this work will focus on the effect of patterning SAF nanodiscs via ion milling, whilst utilising the tunability of the magnetic stack only via its individual layer thicknesses in order to access functional particles, with a variety of switching fields, for applications in liquid.

To investigate how the effect of patterning might impact nanodiscs manufactured for application we grew

a series of PM SAF thin films with different coupling strengths, mediated by the Pt interlayer thickness (t_{Pt}), at the 1st AF coupling peak (AF1) for Ru. They were grown on top of a Ge coated Si substrate in the form $Ta(2)/Pt(2)/CoFeB(0.9)/Pt(t_{Pt})/Ru(0.9)/Pt(t_{Pt})/CoFeB(0.9)/Pt(2)/Ta(2)$ with thicknesses in nm, and where t_{Pt} = 0.37–0.69 nm. They were then patterned into 500 nm discs. The original films and nanodiscs were assessed on chip by MOKE measurements—the hysteresis loops of both sample sets are displayed in Figures 2(a) and (b). Coupling (H_J), coercivity (H_C) and switching fields (H), extracted from the major and minor loops (details included in Section S1 of the supplementary material), are plotted against t_{Pt} in Figures 2(c)–(e).

Both the films and discs exhibit the expected relationship for the coupling field: we find exponentially decreasing H_J with increasing t_{Pt} in Figure 2(c)[21]. Patterning has induced a small reduction in the H_J from films to discs, which is more prominent for smaller t_{Pt}. This

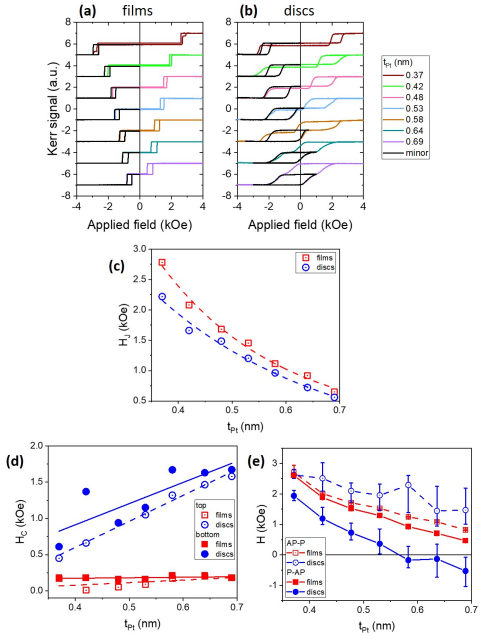

FIG. 2. Major and minor MOKE loops of a PM SAF series with 0.9 nm Ru in (a) thin film and (b) nanodisc form. The variation of (c) coupling field (H_J), (d) top and bottom CoFeB layer coercive fields (H_C), and (e) AP-P and P-AP switching fields with respect to t_{Pt} for the films and nanodiscs. We define the switching field as the middle of each switch, while the error bars represent the start and end points of the transition.

is likely due to a disruption of the PM SAF interlayers (which govern the coupling strength) creating a change in defect distribution in those layers.

The most significant difference between the hysteresis of the thin films and the corresponding sets of nanodiscs is the coercivity of both CoFeB layers, as seen in Figure 2(d). In the case of the switching fields, as seen in Figure 2(e), the change in H_C has lead to the antiparallel-to-parallel (AP-P) switching fields being higher and the parallel-to-antiparallel (P-AP) switching fields being lower for the discs, in addition to the transitions being sloped rather than sharp. Here also, the change in defect distribution (caused by the patterning process) creates a spread of properties across the population of nanodiscs.

There is a positive correlation in H_C with t_{Pt} for both the top and bottom CoFeB layers. We propose that thicker Pt induces stronger PMA, as has been found previously[20]. This will have little impact on the magnetic transitions of the thin films, as they are driven by nucleation and propagation of domains. However, in the case of the nanodiscs, nucleation is required within each individual disc, such that greater PMA yields a greater increase in coercivity upon patterning. In addition, thinner t_{Pt} will affect the change in coercivity from film to nanodiscs through limiting the slope of the transition: thinner Pt leads to an increased quantity of defects in the original film, such that it limits the change in defect distribution during patterning, thus limiting the spread of properties across the nanodisc population. Figure 2(e) clearly shows which nanodisc samples retain their AP remanence state: those that conserve a positive P-AP switching field, namely where $t_{Pt} > 0.55$ nm. This demonstrates the limitation in the fabrication of PM SAF nanodiscs on the more weakly coupled, lower switching end of the spectrum.

An alternative, coarser method for tuning coupling strength is through Ru layer thickness[18,20]. We investigated the potential of accessing functional, lower switching field PM SAF nanodiscs by utilising the 2nd AF coupling peak (AF2). A series of PM SAF films and 500 nm discs were grown in the form $Ta(2)/Pt(2)/CoFeB(0.8)/Pt(t_{Pt})/Ru(2)/Pt(t_{Pt})/CoFeB(0.8)/Pt(2)/Ta(2)$ with thicknesses in nm and where t_{Pt} = 0.21–0.32 nm. The major and minor MOKE loops of these samples are presented in Figures 3(a) and (b), with the extracted coupling, coercivity and switching fields plotted against t_{Pt} in Figures 3(c)–(e).

We observe the characteristic trend of decreasing H_J with increasing t_{Pt}. Additionally, we find a decrease in H_J from films to discs in correspondence with the findings for the AF1 samples.

Overall, we find a similar trend in coercivity from films to discs for the AF2 SAFs as for the AF1 SAFs: a general rise in H_C from films to discs and an increase in H_C with t_{Pt} for the nanodiscs. We do, however, find some variation when we look more closely at the individual layer coercivities of the nanodiscs: the H_C of the bottom

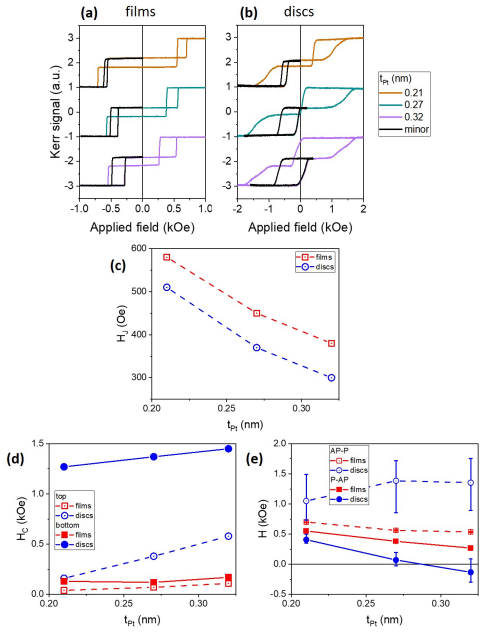

FIG. 3. Major and minor MOKE loops of a PM SAF series with 2 nm Ru in (a) thin film and (b) nanodisc form. The variation of (c) coupling field (H_J), (d) top and bottom CoFeB layer coercive fields (H_C), and (e) AP-P and P-AP switching fields with respect to t_{Pt} for the films and nanodiscs. We define the switching field as the middle of each switch, while the error bars represent the start and end points of the transition.

layer is consistently much higher than that of the top layer. We can attribute this effect to inherent defects due to vertical asymmetry in the stack growth[45,46].

Similarly to the AF1 SAFs, the P-AP switching field has consistently dropped after patterning, producing divergence as t_{Pt} (and thus PMA) increases. Again, this has resulted in the loss of the AP remanence state in the $t_{Pt} = 0.27$ and 0.32 nm samples. However, this state is maintained in the $t_{Pt} = 0.21$ nm sample. This demonstrates that although there is a more restricted range for the production of nanodiscs with a successfully conserved AP state, by using AF2 it is possible to create functional PM SAF nanodiscs that are coupled in the lower field range (and significantly below the ~ 1.2 kOe limit found for the AF1 nanodiscs). Further analysis of the effect of patterning on the AP-P and P-AP transitions is included in Section S4 of the supplementary material.

Significantly, we have seen that large changes in H_C in more weakly coupled SAFs can lead to the loss of the AP remanence state that prevents particle agglomeration. Thus, we found it useful to further probe the impact these changes might have on magnetic particles for applications, namely, those engineered with a particular switching field. By plotting the changes in field parameters with respect to the coupling strength of the films, instead of t_{Pt} (for reference, additional analysis of coercivity versus t_{Pt} is included in Section S4 of the supplementary material), we can study the SAF behaviour through a metric that is more applicable to design for application.

Figures 4(a) and (b) display the results for both change (ΔH_J) and fractional change ($\Delta H_J/H_J$ film) in coupling strength for the AF1 and AF2 SAFs, as we go from films to discs. ΔH_J shows a clear negative correlation with H_J film across the samples. By translating this into a fractional change, and calculating the mean and standard deviation across the full data set, we find that this trend originates from a general change in behaviour caused by patterning. The transformation of a SAF stack from a thin film to nanodiscs generated a percentage decrease in coupling strength of $18 \pm 4\%$ on average.

In Figure 4(c) we see an inverse correlation between change in coercivity (ΔH_C, going from films to discs) and H_J film across the board. As expected from earlier analysis, there is a large increase in ΔH_C from the top (open symbols) to bottom (closed symbols) CoFeB layers in the AF2 (blue) nanodiscs (~ 1000 Oe). The AF1 (red) discs exhibit a more similar range of ΔH_C across the series, with a relatively small rise in value from the top to bottom CoFeB layer (~ 200 Oe). This behaviour has led to a much larger step in ΔH_C from the AF1 to AF2 discs for the top CoFeB layer (> 1000 Oe) compared to the bottom layer. As the top CoFeB layer is inherently further

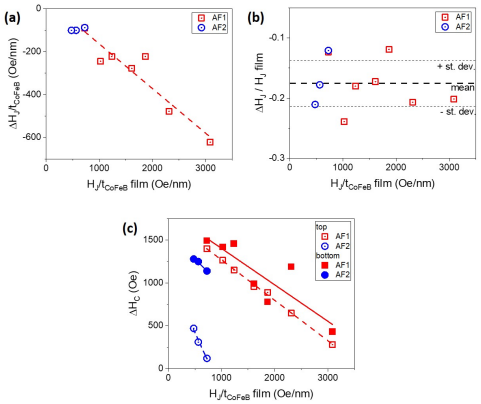

FIG. 4. The (a) change in coupling (re-scaled by CoFeB thickness, t_{CoFeB}), (b) fractional change in coupling, and (c) change in coercivity from films to nanodiscs, with respect to the H_J of the films (re-scaled by t_{CoFeB}). The mean, -0.18, and one standard deviation, 0.04, from the mean are marked by the dashed lines in (b).

away from the Ta smoothing layer (than the bottom layer within the same stack), it will experience greater roughness and defects in its interfaces[45,46]. This effect will be more prevalent the thinner t_{Pt} is (lowest in the AF2 samples), where the greater density of inherent defects will limit the change in defect distribution caused by the patterning process. In addition, we note that thicker t_{Pt} causes a greater coercive increase due to stronger PMA. Overall, this leads to a much smaller change in coercivity in the AF2 discs, which utilise the thinnest Pt interlayers, compared to the weakest coupled AF1 discs.

In summary, these results indicate that the process of patterning a thin film into nanodiscs has a smaller impact on the functional magnetic properties of a lower switching field ($H < 1$ kOe) PM SAF coupled with AF2 than one coupled by AF1. Significantly, this leads to a higher potential for conserving the AP remanence state in more weakly coupled SAF nanodiscs. Thus, if an application requires the use of SAF particles with lower switching fields, and hence lower coupling, it appears to be highly beneficial to utilise AF2 in the multilayer stack.

Figure 5 presents the vibrating sample magnetometry (VSM) measurements of the more weakly coupled AF1 and all AF2 nanodiscs suspended in water, compared to the original thin films. Releasing PM SAF particles into liquid provides them with an additional degree of freedom—mechanical rotation—which alters their magnetic hysteresis response from that observed for the original thin film (or the particles prior to lift off)[16]. The hysteretic behaviour of PM SAF particles in liquid has been thoroughly detailed in our previous study[16], and is summarised in Section S5 of the supplementary material. Namely, the transitions are less sharp due to the spread of coupling and coercivity fields across the particle population, and there is an additional linear response between zero and saturation due to the introduction of a canted regime (see previous study[16]).

The presence of a non-AP remanence state in PM SAF nanodiscs induces additional variation in the hysteresis. This is observed in the liquid VSM loops of all of the AF1 nanodiscs in Figures 5(a)–(c), but is particularly clear in the $t_{Pt} = 0.64$ and 0.69 nm samples. Here, there is a very strong switch through zero field, which results from a 180° rotation of the particles as they realign their moments with the field direction. This is followed by a more moderate response to full saturation. We believe that the overall hysteresis is either the result of a multi-domain state being present in the particles at remanence (a mixture of saturated and unsaturated regions), or of a mixed population of particles where some have an AP remanence state and other do not. These concepts are discussed further in Section S5 of the supplementary material.

In the case of the AF2 nanodiscs, due to the conservation of the AP remanence state (which maintains the stability of the discs in liquid), we find that the $t_{Pt} = 0.21$ and 0.27 nm samples have both produced more regular PM SAF particle responses. The liquid VSM loops in

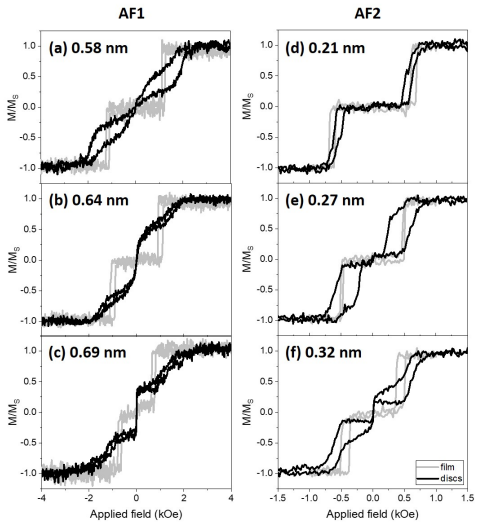

FIG. 5. Liquid VSM loops of (a) the three weakest coupled 1st AF peak nanodiscs samples and (b) the 2nd AF peak nanodiscs samples (black), compared with the original thin films (grey). t_{Pt} is indicated for each sample pair. Each set of nanodiscs was measured at a concentration of $\sim 1 \times 10^9$ particles/ml.

Figures 5(d) and (e) both exhibit a small switch through zero field, which is likely due to a small inherent imbalance in the CoFeB layer moments, as has been discovered previously[16]. The $t_{Pt} = 0.32$ nm nanodiscs (Figure 5(f)) are again experiencing altered behaviour around remanence. We note that the $t_{Pt} = 0.27$ nm nanodiscs did not appear to have maintained their AP remanence state in the MOKE loop as shown in Figure 3(b). The discrepancy here is the result of the magnetic hysteresis being field sweep rate dependent. This is due to the magnetic reversal being a thermally activated process; at low field sweep rate the system spends more time at a particular applied field and therefore has a higher probability of switching magnetically, which induces a lower switching field and thus a lower coercivity. Therefore, with a VSM measurement being taken at a significantly lower field sweep rate than a MOKE measurement, the coercivity is reduced such that the AP remanence state is more likely.

These results demonstrate the conservation of the key magnetic behaviours necessary for functional PM SAFs, in particular low switching fields and an AP remanence state, in nanodiscs that have been released into liquid. They further support the use of AF2 to fabricate nanodiscs for applications that require the implementation of lower applied fields.

We have presented the method for designing PM SAF nanodiscs with a range of switching fields and

investigated how the patterning process affects their magnetic state. Notably, we have demonstrated that the use of the 2nd strongest AF coupling peak allows access to nanodiscs with low switching fields and an AP remanence state. The ability to efficiently and controllably activate particles or generate torque at field strengths below 1 kOe is highly beneficial in applications where it is challenging to apply strong magnetic fields. In particular, lab-on-chip technologies, such as point-of-care devices, need to minimise applied field strengths for both practicality and cost effectiveness.

See the supplementary material for additional information on the PM SAF multilayer structure and magnetic transitions, the nanodisc fabrication method, analysis of the effect of pattern size on PM SAF hysteresis, analysis of switching in AF1 and AF2 PM SAFs, and switching behaviour of PM SAF nanodiscs in liquid.

ACKNOWLEDGMENTS

This work was supported by the Rosetrees Trust.

DATA AVAILABILITY STATEMENT

The data that support the findings of this study are available from the corresponding author upon reasonable request.

[1]Q. A. Pankhurst, J. Connolly, S. K. Jones, and J. Dobson, Journal of Physics D-Applied Physics **36**, R167 (2003).
[2]Q. A. Pankhurst, N. T. K. Thanh, S. K. Jones, and J. Dobson, Journal of Physics D: Applied Physics **42**, 224001 (2009).
[3]T. Neuberger, B. Schöpf, H. Hofmann, M. Hofmann, and B. von Rechenberg, Journal of Magnetism and Magnetic Materials **293**, 483 (2005).
[4]H. Joisten, T. Courcier, P. Balint, P. Sabon, J. Faure-Vincent, S. Auffret, and B. Dieny, Applied Physics Letters **97**, 253112 (2010).
[5]K. K. Narayanasamy, M. Cruz-Acuña, C. Rinaldi, J. Everett, J. Dobson, and N. D. Telling, Journal of Colloid and Interface Science **532**, 536 (2018).
[6]D. Kim, Y. Zhang, W. Voit, K. Rao, and M. Muhammed, Journal of Magnetism and Magnetic Materials **225**, 30 (2001).
[7]Y. Lalatonne, J. Richardi, and M. P. Pileni, Nature Materials **3**, 121 (2004).
[8]A. K. Gupta and M. Gupta, Biomaterials **26**, 3995 (2005).
[9]A. Ali, H. Zafar, M. Zia, I. ul Haq, A. R. Phull, J. S. Ali, and A. Hussain, Nanotechnology, Science and Applications **Volume 9**, 49 (2016).
[10]D.-H. Kim, E. a. Rozhkova, I. V. Ulasov, S. D. Bader, T. Rajh, M. S. Lesniak, and V. Novosad, Nature materials **9**, 165 (2010).
[11]E. A. Vitol, V. Novosad, and E. A. Rozhkova, Nanomedicine **7**, 1611 (2012).
[12]S. Leulmi, H. Joisten, T. Dietsch, C. Iss, M. Morcrette, S. Auffret, P. Sabon, and B. Dieny, Applied Physics Letters **103**, 132412 (2013).
[13]Y. Cheng, M. E. Muroski, D. C. Petit, R. Mansell, T. Vemulkar, R. A. Morshed, Y. Han, I. V. Balyasnikova, C. M. Horbinski, X. Huang, L. Zhang, R. P. Cowburn, and M. S. Lesniak, Journal of Controlled Release **223**, 75 (2016).
[14]T. Vemulkar, R. Mansell, D. C. M. C. Petit, R. P. Cowburn, and M. S. Lesniak, Applied Physics Letters **107**, 012403 (2015).
[15]R. Mansell, T. Vemulkar, D. C. M. C. Petit, Y. Cheng, J. Murphy, M. S. Lesniak, and R. P. Cowburn, Scientific Reports **7**, 4257 (2017).
[16]T. Vemulkar, E. N. Welbourne, R. Mansell, D. C. M. C. Petit, and R. P. Cowburn, Applied Physics Letters **110**, 042402 (2017).
[17]in *Solid State Physics*, edited by R. E. Camley and R. L. Stamps (Academic Press, 2011).
[18]S. S. Parkin, Physical Review Letters **67**, 3598 (1991).
[19]O. Hellwig, A. Berger, J. B. Kortright, and E. E. Fullerton, Journal of Magnetism and Magnetic Materials **319**, 13 (2007).
[20]S. Bandiera, R. C. Sousa, S. Auffret, B. Rodmacq, and B. Dieny, Applied Physics Letters **101**, 072410 (2012).
[21]R. Lavrijsen, A. Fernández-Pacheco, D. Petit, R. Mansell, J. H. Lee, and R. P. Cowburn, Applied Physics Letters **100**, 052411 (2012).
[22]R.-J. Yang, H.-H. Hou, Y.-N. Wang, and L.-M. Fu, Sensors and Actuators B: Chemical **224**, 1 (2016).
[23]C. P. Moerland, L. J. Van IJzendoorn, and M. W. Prins, Lab on a Chip **19**, 919 (2019).
[24]E. Rapoport and G. S. Beach, Scientific Reports **7**, 17 (2017).
[25]E. N. Welbourne, T. Vemulkar, and R. P. Cowburn, Nano Research **12**, 0 (2021).
[26]M. T. Johnson, P. J. H. Bloemen, F. J. A. den Broeder, and J. J. de Vries, Reports on Progress in Physics **59**, 1409 (1996).
[27]T. Vemulkar, R. Mansell, D. C. M. C. Petit, R. P. Cowburn, and M. S. Lesniak, Journal of Applied Physics **121**, 043908 (2017).
[28]J. C. Read, P. M. Braganca, N. Robertson, and J. R. Childress, APL Materials **2**, 046109 (2014).
[29]N. Persat and A. Dinia, Phys. Rev. B **56**, 2676 (1997).
[30]W. Alayo and E. Baggio-Saitovitch, Journal of Applied Physics **107**, 73909 (2010).
[31]Y. Zhu, Z. Zhang, B. Ma, and Q. Y. Jin, Journal of Applied Physics **111**, 07C106 (2012).
[32]Y. Li, X. Jin, P. Pan, F. N. Tan, W. S. Lew, and F. Ma, Chinese Physics B **27**, 127502 (2018).
[33]R. Hyndman, P. Warin, J. Gierak, J. Ferré, J. N. Chapman, J. P. Jamet, V. Mathet, and C. Chappert, Journal of Applied Physics **90**, 3843 (2001).
[34]C. Fowley, Z. Diao, C. C. Faulkner, J. Kally, K. Ackland, G. Behan, H. Z. Zhang, A. M. Deac, and J. M. D. Coey, Journal of Physics D: Applied Physics **46**, 195501 (2013).
[35]T. A. Moore, I. M. Miron, G. Gaudin, G. Serret, S. Auffret, B. Rodmacq, A. Schuhl, S. Pizzini, J. Vogel, and M. Bonfim, Applied Physics Letters **93**, 262504 (2008).
[36]T. Thomson, G. Hu, and B. D. Terris, Physical Review Letters **96**, 1 (2006).
[37]J. M. Shaw, M. Olsen, J. W. Lau, M. L. Schneider, T. J. Silva, O. Hellwig, E. Dobisz, and B. D. Terris, Physical Review B - Condensed Matter and Materials Physics **82**, 1 (2010).
[38]J. M. Shaw, S. E. Russek, T. Thomson, M. J. Donahue, B. D. Terris, O. Hellwig, E. Dobisz, and M. L. Schneider, Physical Review B **78**, 024414 (2008).
[39]V. Baltz, A. Bollero, B. Rodmacq, B. Dieny, J.-P. Jamet, and J. Ferré, The European Physical Journal - Applied Physics **39**, 33 (2007).
[40]R. P. Cowburn, Journal of Physics D: Applied Physics **33** (2000), 10.1088/0022-3727/33/1/201.
[41]M. S. Pierce, J. E. Davies, J. J. Turner, K. Chesnel, E. E. Fullerton, J. Nam, R. Hailstone, S. D. Kevan, J. B. Kortright, K. Liu, L. B. Sorensen, B. R. York, and O. Hellwig, Physical Review B - Condensed Matter and Materials Physics **87**, 1 (2013), arXiv:1301.1737.
[42]Y. Liu, L. Hao, and J. Cao, AIP Advances **6** (2016), 10.1063/1.4947132.
[43]C. Burrowes, N. Vernier, J.-P. Adam, L. Herrera Diez, K. Garcia, I. Barisic, G. Agnus, S. Eimer, J.-V. Kim, T. Devolder, A. Lamperti, R. Mantovan, B. Ockert, E. E. Fullerton, and D. Ravelosona, Applied Physics Letters **103**, 182401 (2013).

[44]S. Srivastava, A. P. Chen, T. Dutta, R. Ramaswamy, J. Son, M. S. M. Saifullah, K. Yamane, K. Lee, K.-L. Teo, Y. P. Feng, and H. Yang, Physical Review Applied **10**, 024031 (2018).
[45]J. H. Lee, R. Mansell, D. Petit, A. Fernández-Pacheco, R. Lavrijsen, and R. P. Cowburn, SPIN **03**, 1340013 (2013).
[46]D. Petit, R. Lavrijsen, J. Lee, R. Mansell, A. Fernández-Pacheco, and R. P. Cowburn, Nanotechnology **27** (2016), 10.1088/0957-4484/27/15/155203.

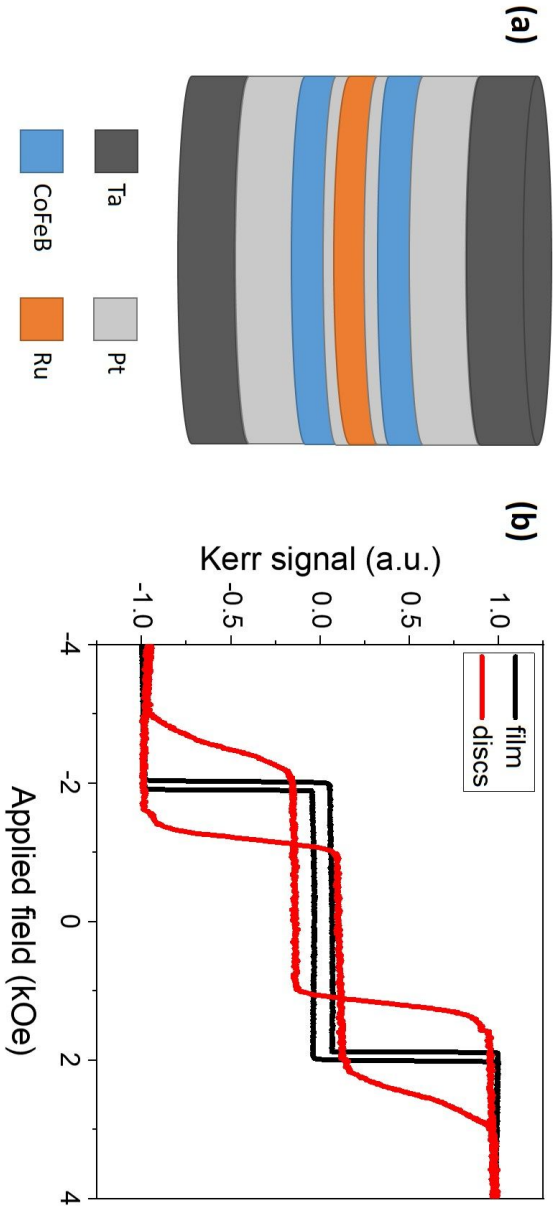

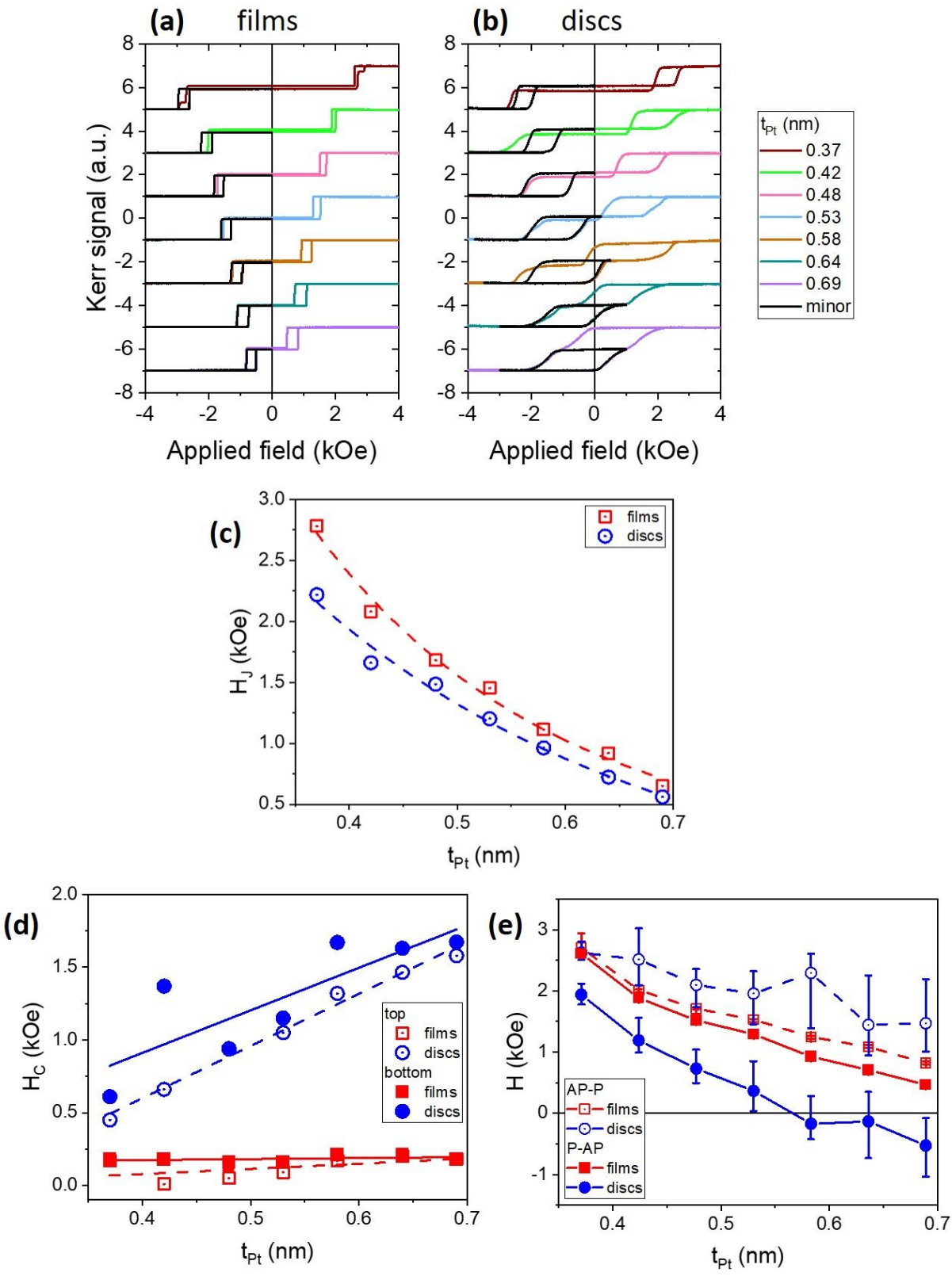

Applied Physics Letters